





Warm surface waters increase Antarctic ice shelf melt and delay dense water formation

Shigeru Aoki ^{1,2✉}, Tomoki Takahashi², Kaihe Yamazaki^{1,2}, Daisuke Hirano ^{3,4}, Kazuya Ono ¹, Kazuya Kusahara⁵, Takeshi Tamura ^{3,4} & Guy D. Williams⁶

Melting ice shelves around Antarctica control the massive input of freshwater into the ocean and play an intricate role in global heat redistribution. The Amery Ice Shelf regulates wintertime sea-ice growth and dense shelf water formation. We investigated the role of warm Antarctic Surface Water in ice shelf melting and its impact on dense shelf water. Here we show that the coastal ocean in summer 2016/17 was almost sea-ice free, leading to higher surface water temperatures. The glacial meltwater fraction in surface water was the highest on record, hypothesised to be attributable to anomalous ice shelf melting. The excess heat and freshwater in early 2017 delayed the seasonal evolution of dense shelf water. Focused on ice shelf melting at depth, the importance and impacts of warming surface waters has been overlooked. In a warming climate, increased surface water heating will reduce coastal sea-ice production and potentially Antarctic Bottom Water formation.

¹Institute of Low Temperature Science, Hokkaido University, Sapporo, Japan. ²Graduate School of Environmental Science, Hokkaido University, Sapporo, Japan. ³National Institute of Polar Research, Tachikawa, Tokyo, Japan. ⁴The Graduate University for Advanced Studies, Tachikawa, Tokyo, Japan. ⁵Japan Agency for Marine-Earth Science and Technology, Yokosuka, Japan. ⁶University of Tasmania, Hobart, Australia. ✉email: shigeru@lowtem.hokudai.ac.jp

The Antarctic margin and continental shelf globally impact the heat, freshwater, and carbon cycles through the global thermohaline circulation¹. Acceleration of continental ice mass loss, initiated through the melting of ice shelves by oceanic heat, will additionally lead to a rise in global mean sea level^{2–4}. Excess glacial meltwater input alters stratification that can induce a change in the ventilation of Antarctic Bottom Water^{5–7}, the densest watermass in the global ocean. The variability in coastal stratification can also change air-sea exchange of carbon-dioxide and biological productivity^{8,9}. Antarctic shelf waters vary regionally depending the interaction of key physical processes such as buoyancy loss through sea water freezing, heat supply by warm water intrusion, and freshwater discharge from continental ice^{10,11}. Antarctic Bottom Water broadly forms from Dense Shelf Water (DSW)^{12,13} that originates from sea-ice production and brine rejection in polynyas around the Antarctic coast¹⁴. The second largest polynya, as defined by the area of sea-ice production¹⁴, is the Cape Darnley Polynya (CDP, Fig. 1a). The CDP is located immediately west of a large continental embayment called Prydz Bay (PB; Fig. 1a), into which flows the Lambert Glacier–Amery Ice Shelf (AIS), the largest glacier–ice-shelf system in East Antarctica¹⁵. Ocean circulation in this embayment is characterized by the clockwise Prydz Bay Gyre associated with westward coastal current, which transports warm modified Circumpolar Deep Water shoreward^{16,17}. Downstream and upstream of the AIS are the Mackenzie and Barrier Polynyas, which provide substantial brine rejection and DSW formation¹⁸. Traditionally, the AIS has been regarded as a cold cavity system, with its glacial melting mainly driven by DSW as the Deep Mode and to a lesser extent by modified Circumpolar Deep Water as the Intermediate Mode^{19,20}, out of the typical three overturning circulation regimes in sub-ice-shelf cavity^{21,22}.

The meltwater discharged from ice shelves can affect the neighboring oceanic environment. Ice Shelf Water from the AIS tempers the efficacy of the local polynyas^{18,23}. As for the remaining Shallow Mode, driven by the atmospheric heating of Antarctic Surface Water (AASW) that subsequently interacts with the shallower regions of an ice shelf, the effect is considered to be limited and has been largely disregarded. Recently, from the in-situ ice radar measurements and nearby oceanic observations, it is shown that the summer AASW induces prominent basal melt of the Ross Ice Shelf^{24,25}. However, the processes of oceanic surface heating and impact of the resultant meltwater on the adjacent ocean has not been investigated yet.

This study examines the year-round effect of continental ice melt on watermass properties in the PB/CDP system, based on in-situ observations of the latter half of 2010s, including those by originally developed moored profiling platforms at CDP (Fig. 2 and Supplementary Fig. 1). Specifically, the behavior of glacial meltwater fraction in seawater discerned using the stable oxygen isotope ratio ($\delta^{18}\text{O}$) obtained by ship-board and time-series water samplings. Satellite observations are used to describe oceanic and sea-ice spatial structure, together with a numerical simulation incorporating the process of ice shelf melt. In concert, we identified a series of phenomena in the 2017 season that characterizes the interaction between ocean, sea ice, and continental ice in an anomalously warm climate condition that could be prevalent in future climate.

Results and discussion

Warmer surface water and extra meltwater in summer 2017. Summer sea surface temperature (SST) across the Antarctic sea-ice zone varies interannually. In February 2017, satellite-derived SST²⁶ was anomalously warm over the PB/CDP system (Fig. 1a). At CDP, observed ocean profiles (Methods) revealed that the

temperature at 0–100 m depths was ~ 0.5 – 1°C warmer in 2017 compared to the other years (Fig. 1b). Concurrently, $\delta^{18}\text{O}$ was distinguishably lower (-0.55 – -0.6‰) when compared to four years of available data (-0.4 – -0.5‰ ; Fig. 1c). A lower $\delta^{18}\text{O}$ indicates a higher fraction of glacial meltwater²⁷ (Methods section). The glacial meltwater fraction was 1.3% for the lower bound and 1.9% for the upper bound at 50 m depth in February 2017 (Fig. 1d; Methods section; and Supplementary Fig. 3), which was the highest over the four years measured and higher by $0.5 \pm 0.1\%$ ($\sim 30\%$ of total) for both lower and upper limits. The warm water layer with high glacial meltwater fraction in 2017 was not just observed for CDP but also for the shelf break off CDP (Fig. 1e, f, g), which indicates that the higher meltwater content observation was robust and broadly distributed.

According to the satellite-based estimates of summer (average from December through February) SST and sea-ice concentration (SIC)²⁸, the 2017 summer was warm with high SST and low SIC (Fig. 3a, b). In fact, at the CDP there was no sea ice on 26 February 2017 at the time of our core observations but it was mostly ice-covered a year later (Fig. 2). Although the direct evidence of excessive glacial meltwater was observed only in 2017, the situation in 2017 might be considered as a typical example of future summers in a warming climate.

Warm surface water causes upper basal melt of Amery Ice Shelf. The warm summer state with high SST and low SIC in the CDP was wide-spread for the entire PB (Fig. 1a). Satellite time series reveal the basin-scale interannual co-variabilities between the SST and SIC (Fig. 3a, b). Defining warm summers based on the spatially averaged summer SST of the AIS region (Fig. 3e), the five warmest summers after 2000 are 2001, 2003, 2004, 2010, and 2017. The relationship between high SST and low SIC averaged from December through February is statistically robust (two-sided 1% level of significance) with a correlation coefficient of -0.82 (-0.77) for the PB (AIS) region over the 35 years from 1986–2020. The relationship could be explained by the open water/ice-albedo feedback²⁹, whereby less sea ice enhances the surface heat input by solar radiation, leading to further reduction in sea ice.

The solar heat input is not confined at the surface but transported deeper into the water column in front of AIS. Temperature profiles in February 2017 revealed a thick layer of warmer AASW, extending well below the ice shelf draft depth of 250 m³⁰ and much deeper compared with hydrographic data in other years (Fig. 1h). A density surface delineating warm AASW ($\sigma_\theta = 27.72 \text{ kg m}^{-3}$) was relatively shallow offshore and deeper near the ice front of the AIS in both observations and our numerical model. The density surface of AASW gets progressively deeper near the AIS and exceeds the draft depth in the numerical model (Supplementary Fig. 4). The AASW layer thicker than 250 m has been commonly observed at the AIS ice front²⁰. The prevailing coastal easterly wind transports warm AASW shoreward and converges it in front of AIS. This process of Ekman coastal convergence has been commonly detected in this ocean sector off East Antarctica^{31,32}. Once the warm AASW converges towards the ice front and the depth exceeds the draft of the ice shelf front, it can subduct into the cavity beneath the ice shelf and supply heat for the basal melt, which is more impactful than lateral melt^{25,31}.

Our numerical simulation replicates the features of the warm 2017 summer in PB, together with the realistic timing of interannual variabilities of SST and SIC (Supplementary Fig. 5). In representing the ice shelf processes, the model produces higher basal melt at the front of the AIS in 2017 and in other warm summers (Fig. 3c), suggesting the correspondence with warmer

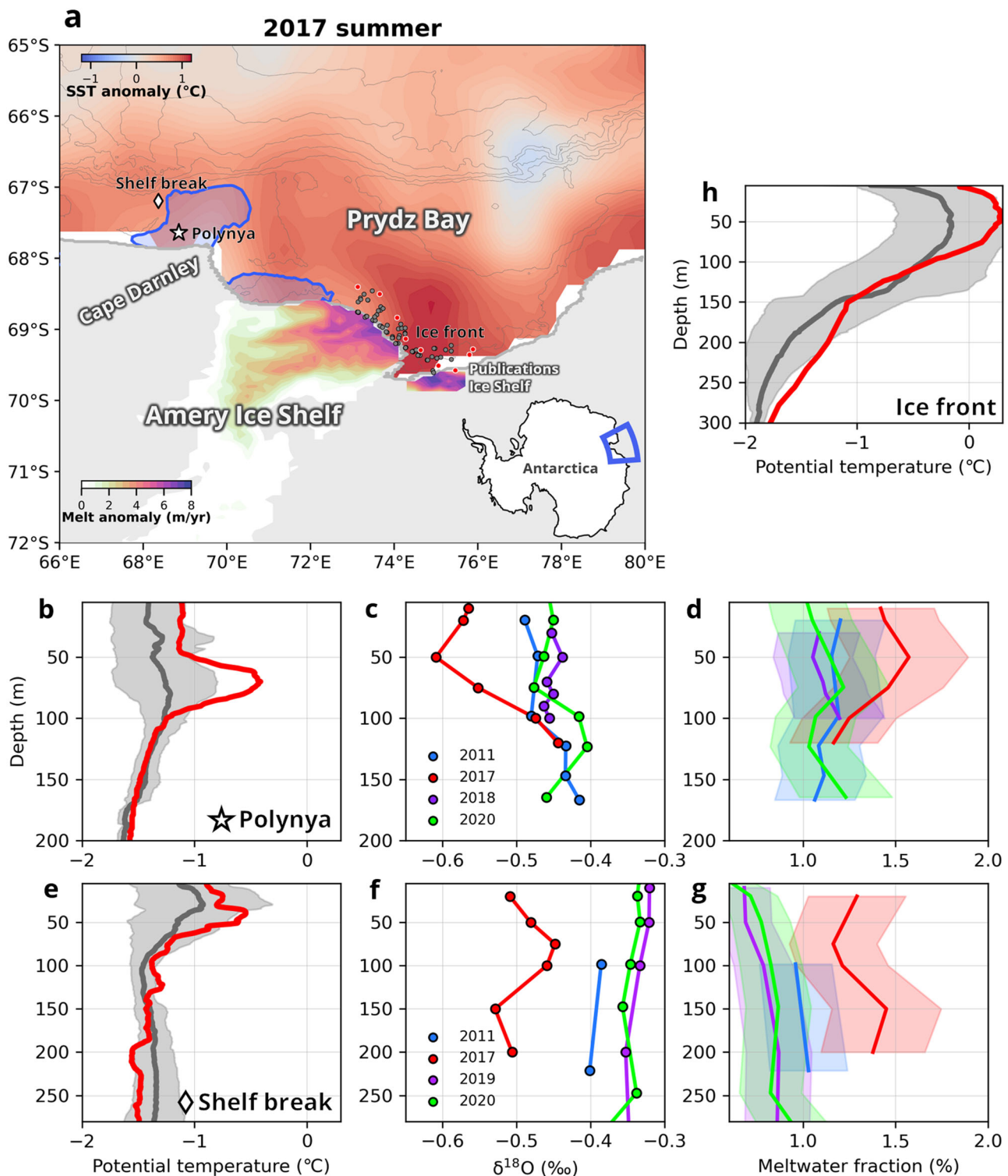


Fig. 1 Anomalously warm summer in 2017. **a** Distribution of sea surface temperature (SST)²⁶ anomaly in February 2017. Active polynyas (climatological sea ice production above 10 m yr^{-1})⁵¹ are shown in blue. Model-based melt rate anomaly in 2017 (relative to the 1979–2019 climatology) is shown for the Amery Ice Shelf and Publications Ice Shelf. **b**, **e**, **h** Vertical profiles of potential temperature from summer hydrography **b** in the Cape Darnley Polynya (CDP), **e** at the shelf break off CDP, and **h** in front of Amery Ice Shelf. Red solid line denotes the station average in February 2017 shown by red dots in **a**, and the gray solid line denotes the station average in February during 2010–2020 shown by all dots in **a**, respectively. Profiles are first averaged for each year, and then averaged for all years. Gray error bar indicates the standard deviation of the multiple years. **c**, **f** Vertical profiles of oxygen isotope ratio and **d**, **g** profiles of glacial meltwater fraction (**c**, **d**) off CDP and (**f**, **g**) at the shelf break off CDP. The upper-bound and lower-bound of the meltwater fraction in **d**, **g** were derived from the oxygen isotope endmember of iceberg and ice-core, respectively, and the solid line denotes their average.

SST. The simulated summer basal melt was especially large at the eastern front of the AIS (Fig. 1a), consistent with the distribution of high SST and warm AASW at depth (Supplementary Fig. 6).

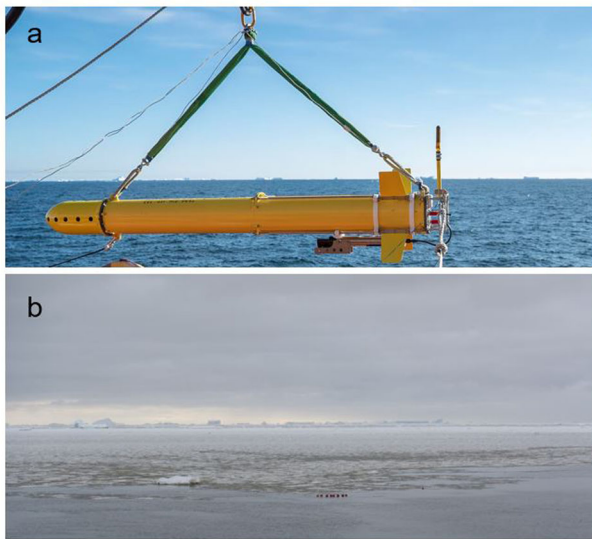


Fig. 2 Oceanic states at Cape Darnley Polynya and the deployed tethered Ocean Observing System-1 profiler. **a** Oceanic state on 26 February 2017 during warm summer and **b** on 26 February 2018 of normal summer.

The basal melt rate near the ice shelf front of AIS/Publication Ice Shelf (PIS) (north of 70°S) at 73°E exceeded 6 m month⁻¹ in February 2017 and was the highest during the 40-year model period (Figs. 1a and 3c; and Supplementary Fig. 7). The cumulative meltwater volume for the 2017 summer (January–May) was 22.6 Gt (Fig. 3c) near the ice shelf front, which was 12.7 Gt greater than the climatological mean (9.9 Gt). The annual (January–December) meltwater volume derived from the total AIS/PIS area was the highest (69.2 Gt) in 2017, 18.9 Gt greater than the climatological mean (50.3 Gt). Hence, more than half of the excess melt in 2017 was contributed by the anomalous summer melt near the ice shelf front, which was estimated to be greater than 20% of the total meltwater from the entire AIS/PIS.

We obtained over-winter mooring records of CDP glacial meltwater fraction derived from $\delta^{18}\text{O}$, temperature/salinity profiles, and current velocity in 2017 (Fig. 4). The time series of glacial meltwater fraction at 176 m depth revealed the high values observed in summer continued to early winter around June (Fig. 4a). With the current speed estimate (4.3 cm s⁻¹) averaged over the four months from March to June (Supplementary Fig. 2), the cumulative transport distance (between the start and end of the progressive vector for the four months) was estimated to be about 450 km. The distance is much longer than the distance between the AIS and CDP, which underpins the influence of advection from the AIS. The volume of melt water is estimated to be about 13.5 Gt by multiplying the meltwater fraction anomaly of 0.5%, derived from the $\delta^{18}\text{O}$ hydrography and mooring, with a total volume flux of a 100 m water column height, 60 km width

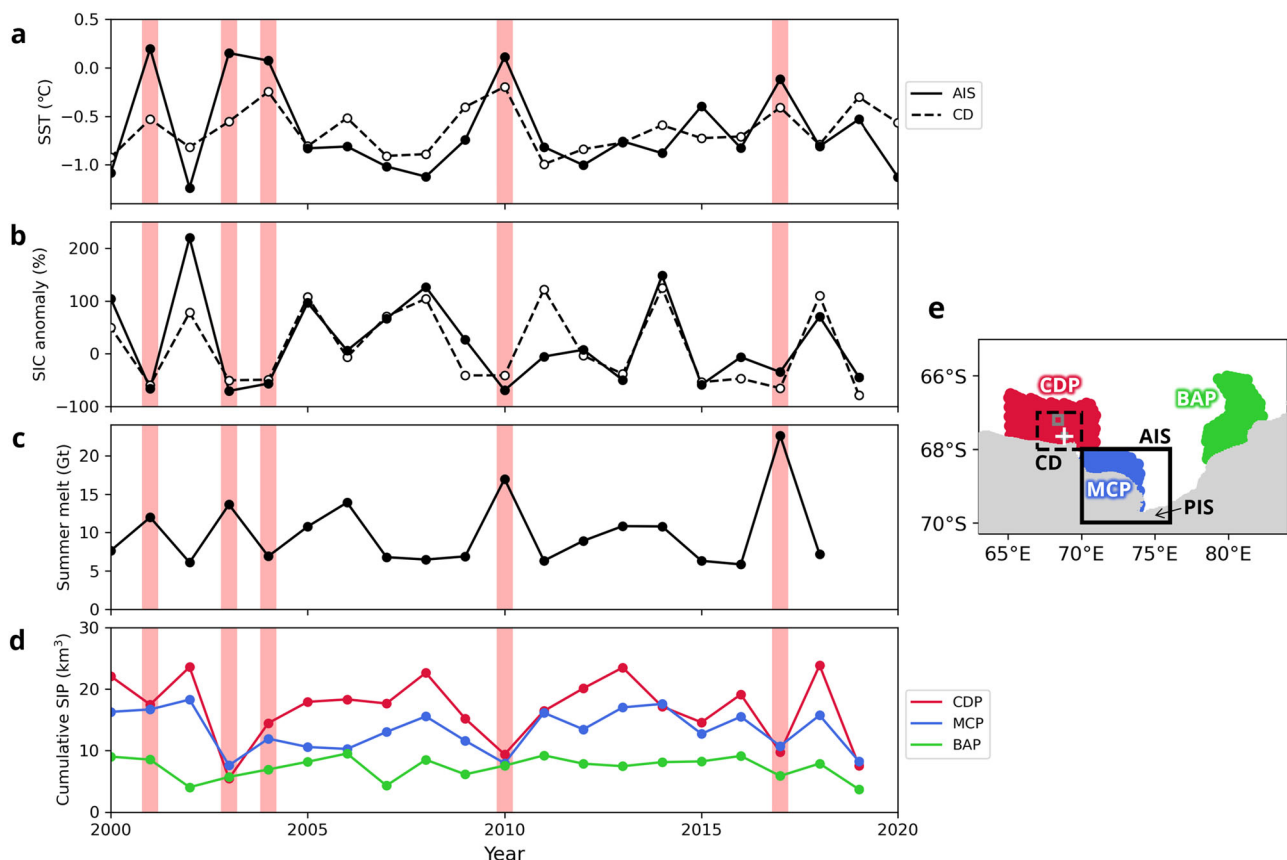


Fig. 3 Interannual variations of sea surface temperature (SST), sea ice concentration, and simulated continental ice melt. **a** Time series of summer (DJF)-averaged SST in Amery Ice Shelf (AIS; solid) and Cape Darnley Polynya (CDP; dashed). Warm years including 2017 are indicated by red shading. **b** Anomaly of summer-averaged sea-ice extent (in %; normalized by the climatological mean). **c** Summer glacial melt near the ice front of the AIS/PIS (north of 70°S; from January to May). **d** Initial cumulative sea-ice production (from Day of Year 0 to 80) in CDP, Mackenzie Polynya (MCP), and Barrier Polynya (BAP). The corresponding locations are indicated in panel **e**, where solid and dashed rectangles are AIS and CDP, respectively.

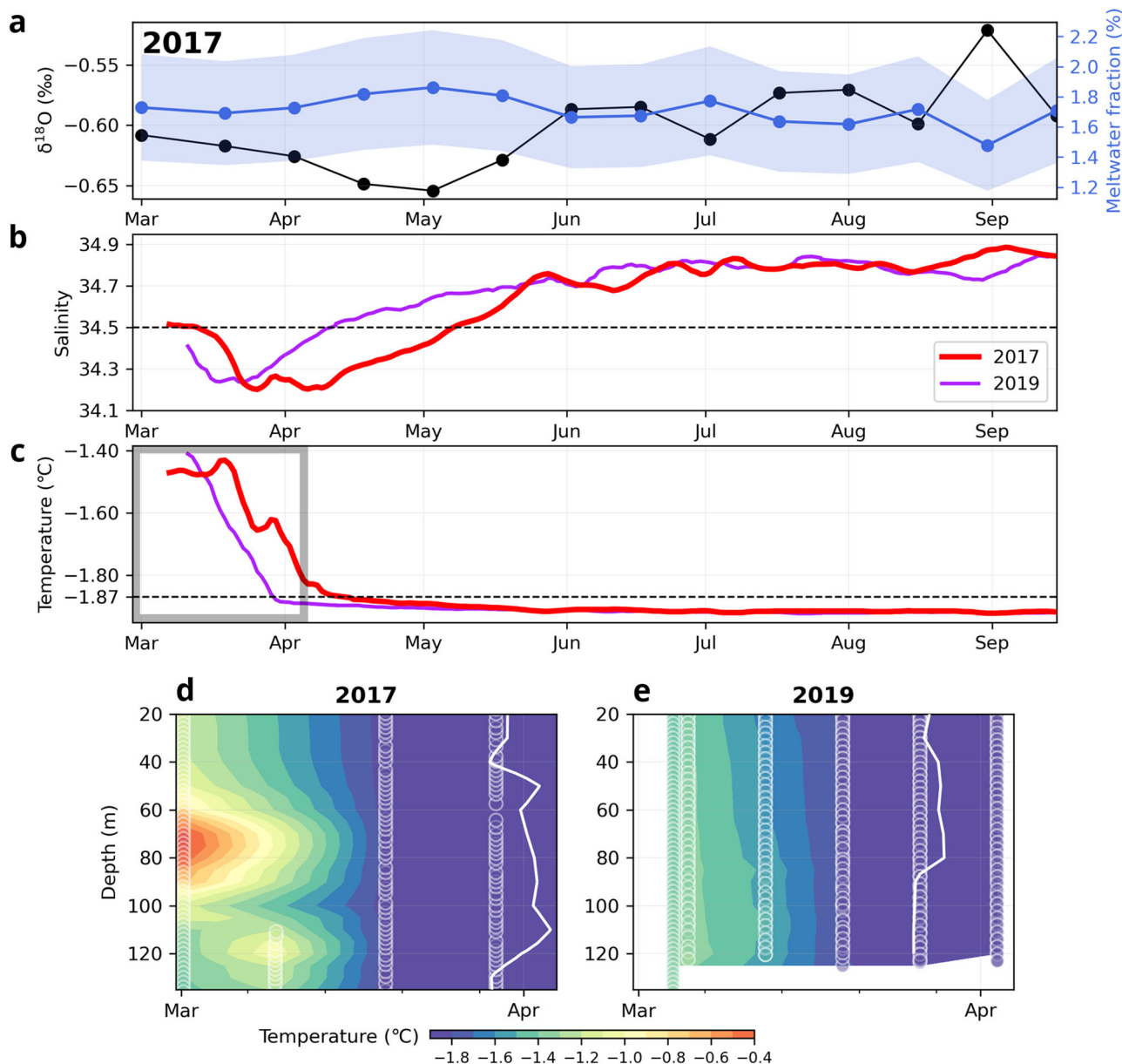


Fig. 4 Seasonal evolution of water properties at CDP. **a** Oxygen isotope ratio (black) and glacial melt water fraction (blue) in 2017, which was derived from three-point endmember method. **b**, **c** are seven-day running mean timeseries of salinity and temperature at 164 m depth in 2017 (red) and 2019 (purple). Broken line at 34.5 in **b** denotes the salinity criteria of DSW, and that at -1.87 °C in **c** denotes the freezing point temperature at a reference salinity in autumn. **d**, **e** are the time-depth plots for temperature (color shade) during the period of onset of freezing indicated in **c**, obtained from the mooring platforms. Data points are shown by scatters. White contour corresponds to the isotherm of -1.87 °C as a reference temperature. The location of the measurements is indicated by the white cross in Fig. 3e.

from CDP to shelf break, and 450 km distance. The consistency of this estimation with the modeled summer melt anomaly at the AIS terminus (12.7 Gt) supports the idea that the abnormally high fraction of continental basal meltwater at the CDP originated from the AIS.

The volume of basal meltwater obtained in this study is comparable to previous estimates. The area-total basal meltwater of the AIS has been estimated as 27 and 52 Gt yr^{-1} based on in situ measurements^{33,34}, 36 Gt yr^{-1} using satellite measurements³⁵, and 46 Gt yr^{-1} by a numerical model¹⁹. In general the volume of basal meltwater was much larger than that of surface meltwater runoff. According to a recent estimate of runoff volume at the AIS, surface melt was high during the 2016/17 summer with a volume few times larger than ordinary summers³⁶. However, their peak volume was

estimated as <1 Gt, significantly smaller than the basal melt by an order of magnitude. Hence the volume of glacial meltwater discharged into the nearby ocean is dominated by the basal melting of AIS/PIS.

Delayed dense water formation at Cape Darnley Polynya. The presence of widespread warm AASW and a large amount of meltwater input in summer/autumn can impact the formation of DSW in the subsequent autumn/winter by determining the onset of sustained sea-ice growth and properties of the new winter mixed layer. At CDP, time series of ocean temperature profiles in autumn 2017 revealed about a week delay in near-surface cooling compared with autumn 2019 (Fig. 4d, e). The temperature at

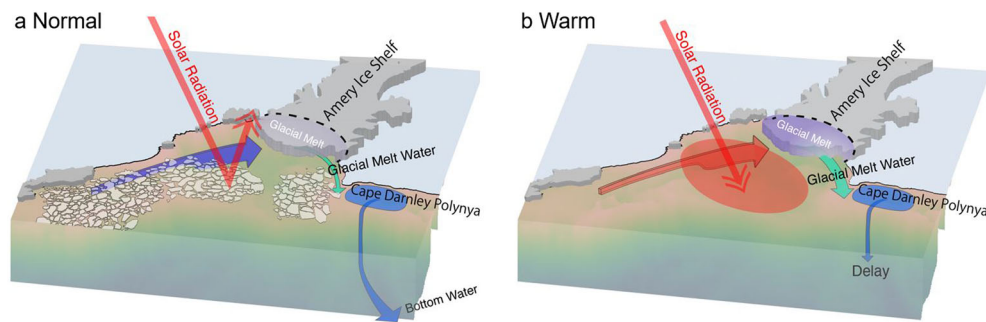


Fig. 5 Schematic oceanic and cryospheric state in the Prydz Bay and off Cape Darnley. a Climate condition in normal summers and subsequent dense shelf water formation in early-winter and **b** those in warm summers.

164 m depth was above freezing until mid-April in 2017, while in 2019 the temperature at the same depth reached freezing point in late-March (Fig. 4c), showing a few-week delay in 2017. The result suggests that the warmer AASW in 2017 delayed the onset of freezing at CDP.

Independent observational evidence concurs that the initiation of sea-ice production was impacted by the warmer AASW in 2017. Based on satellite-derived sea-ice production (SIP), cumulative SIP at CDP until mid-March (day 80) in 2017 was the third smallest among the two decades after 2000 (Fig. 3d). Using a cumulative SIP criterion of 15 km^3 , we find this threshold was reached about one week later in 2017 (and across five other warm summer) relative to the average summers across 2000–2020. For example, the cumulative SIP (day 80) in the five warm years revealed less sea ice production in CDP (statistically significant at two-sided 10% level; Supplementary Fig. 8). The cumulative SIP (day 80) in the Mackenzie and Barrier Polynyas (see Fig. 3e for their locations) also revealed less production in the warm years, although they were statistically insignificant. The synchronous delay in sea-ice production among the three polynyas indicates that the excessive summer heat storage in PB leads to late sea-ice production on a basin scale.

While the excess heat clearly tempers the sea-ice production, just how influential was the basal meltwater from AIS to the evolution of DSW? If we examine the timing of shelf waters reaching 34.5, which is a criterion of DSW in this region¹⁸, then the observed increase in salinity from autumn to early-winter was slower in 2017 by about three weeks compared with another year-round mooring deployed at CDP in 2019 (Fig. 4b). The initial sea-ice production in CDP was relatively small in autumn 2017, but it was even smaller in autumn 2019 (Fig. 3d), indicating the initial salinity increase due to sea-ice production should be faster in 2017 than 2019 and yet this does not entirely correspond with the salinity evolution. Hence the slower salinity increase in 2017 must result from other sources of freshwater, very likely due to the glacial meltwater advected from the AIS.

These results indicate that excess heat storage in summer AASW in PB triggers additional glacial meltwater from the Amery Ice Shelf and that subsequent advection in autumn/early-winter of this freshening causes a delay of about three weeks in the emergence of DSW in the CDP. The three-week delay corresponds to a loss of ~0% of the duration of DSW formation in CDP across March to October.

Implications for future Antarctic surface water. We have demonstrated the excess heat can accelerate the summer melt of ice shelves and delay dense shelf water formation. The beginning of 2017 was a warm summer in PB and the CDP that was likely attributable to the ocean/ice-albedo feedback. In fact, the sea-ice extent in the preceding spring was the minimum across the 40-

year record on the circumpolar scale^{37,38} and contributed to an albedo decrease on a global scale³⁹. The sea-ice extent minimum coincided with anomalously warm Antarctic Surface Water surrounding most of Antarctica^{40,41}. Future predictions of the Southern Ocean indicate a broad loss of sea-ice cover in association with global warming^{42,43}. The series of anomalous phenomena in the 2016/17 season is categorized as just one extraordinary mode at the moment, but the situation delineated in this study could be the new normal in the near future (Fig. 5).

Together with the anomalous surface heating, the excessive glacial meltwater flux induced by warm Antarctic Surface Water can delay dense water formation, suggesting a potential impact on subsequent Antarctic Bottom Water formation. Given the likely increase in open-water/ice-free periods and corresponding surface ocean heat storage around the Antarctic coastline in response to global warming, there will be an step-increase in the importance and impact of Shallow Mode ice shelf melting⁴⁴. The summer heat storage in the Antarctic coastal ocean will thus be of increasing relevance to project both global meridional overturning circulation and sea level rise.

Methods

In situ and satellite observations. We examined in situ ocean observation and satellite-derived sea surface temperature and sea-ice datasets. The ocean observations mainly came from ship-board hydrography and mooring observation outcomes from Japanese Antarctic Research Expedition (JARE) centered at CDP. Ship-board observations were conducted across eight seasons during 2010–2020 (Supplementary Table 1) and consisted of CTD and X-CTD, with occasional Rosette Multi-bottle Sampler for stable oxygen isotope ratio ($\delta^{18}\text{O}$; Supplementary Information). Instrument accuracy is listed in Supplementary Table 2. $\delta^{18}\text{O}$ was available for four years for CDP regions. One station for $\delta^{18}\text{O}$ was occupied each observational year for both CDP and shelf break off CDP. The $\delta^{18}\text{O}$ samples were processed by Finnigan Delta Plus at Institute of Low Temperature Science, Hokkaido University.

Mooring observations were conducted for 2017–2018 and 2019–2020 in CDP at a depth of around 200 m (Supplementary Information). In each year we deployed an originally developed profiler; a buoyancy-driven tethered mid-depth float targeted for 20–180 m during March–October 2017 and a winch-driven mid-depth float targeted for 20–120 m during March–April 2019 (Supplementary Fig. 2). We also deployed an in-situ time-series water sampler (Remote Access Sampler (RAS-500); McLANE Research Laboratories Inc.) during February 2017 – February 2018, equipped with a current meter, and obtained continuous $\delta^{18}\text{O}$ at 150 m depth at 15-day intervals. These samples were processed by Finnigan Delta Plus at the Institute of Low Temperature Science. In 2019 we also collected temperature/salinity data from a sensor attached above the acoustic releaser.

Hydrographic observations used for PB also include the temperature and salinity profiles of the World Ocean Database⁴⁵ and Marine Mammals Exploring the Oceans Pole to Pole (MEOP)-biologging data⁴⁶. MEOP biologging profiles were available in the eastern part of AIS in 2017 and only the most realistic files were used after visual inspection and broad comparison with representative ship-based profiles. For seven seasons during 2001–2017 period, 78 profiles in February were corrected and used. Nine profiles were available in February 2017.

Spatial distributions of monthly SST and SIC were based on satellite measurements. SST data derived from Optimum Interpolation Sea Surface Temperature (OISST) v2.1 High Resolution Dataset provided by National Centers for Environmental Information/ National Oceanic and Atmospheric Administration (NOAA) were used²⁶. The dataset was available for the 1982–2020

period. SIC data derived from Nimbus-7 SMMR and DMSP SSM/I-SSMIS Passive Microwave Data v1 provided by National Snow and Ice Center were used²⁸. The dataset was used for the 1986–2019 period. To calculate the anomalies of SST and SIC, the full data period above was used to calculate their temporal averages.

Estimation of continental ice melt water using stable oxygen isotope ratio.

$\delta^{18}\text{O}$ is a useful tracer in quantifying the origins of freshwater, especially that of glacial meltwater²⁷. Other tracers such as temperature and/or noble gases can be used^{47,48}, but $\delta^{18}\text{O}$ is especially useful near the surface since other tracers are often contaminated from surface exchange processes.

We applied a three-endmember method (glacial meltwater, sea ice, and modified Circumpolar Deep Water⁴⁹; Supplementary Fig. 3) using salinity and $\delta^{18}\text{O}$ to derive the glacial meltwater fraction based on the large difference in $\delta^{18}\text{O}$ between glacial meltwater and sea ice⁵⁰. The largest uncertainty of the fraction estimates originates in the determination of the $\delta^{18}\text{O}$ endmember of the glacial meltwater. To derive lower- and upper- bounds of the glacial estimates, we use the observed estimates of ice cores of AIS (–40‰) and icebergs taken off Cape Darnley (–27‰; Supplementary Information). The $\delta^{18}\text{O}$ and salinity endmembers of sea ice were set as –1.3‰ and 5, respectively, as the averages of the two samples taken at CDP. The $\delta^{18}\text{O}$ and salinity endmembers of modified Circumpolar Deep Water were estimated as –0.078‰ and 34.67, respectively, based on the water samples collected on the continental slope.

Estimation of sea-ice production. We used a sea-ice production (SIP) dataset derived from special sensor microwave/imager (SSM/I) and special sensor microwave imager/sounder (SSMIS) data and atmospheric reanalysis with the ERA5 dataset. Sea-ice production data are seamlessly available for the 28 years during 1992–2019 to examine its variability. This dataset is fundamentally the same as that presented by ref. ⁵¹, with a different atmospheric forcing (ERA5 data are used).

Numerical ocean-sea ice-shelf model. We used an ocean-sea ice model with an ice shelf component⁵². The model configuration is almost the same as in ref. ⁴⁴, but with a higher horizontal resolution and different surface boundary conditions. The horizontal resolution varies from 2.5 km at the southernmost grid cells at 83.5°S to 21 km at the northernmost grid cells at 20°S. The model was driven by atmospheric surface boundary conditions. The daily surface boundary conditions were derived from a climatological surface condition⁵³ and the ERA-Interim dataset using the bulk formula⁵⁴.

The model first spun up for 50 years with the climatological sea surface boundary conditions, and then was integrated for 20 years repeatedly with the 1979 surface boundary conditions derived from the ERA-Interim dataset. Finally, we performed a hindcast simulation for the period 1979–2018 with ERA-Interim's temporally varying surface boundary conditions. This study utilizes monthly-averaged values for analysis. The ice-shelf basal melt rate was diagnosed with the thermodynamic ocean-ice shelf interaction based on the three-equation formulation^{55,56}. The ice shelf and ocean in the model exchange freshwater and heat associated with the diagnosed basal melt rate.

The model in this study reproduces Antarctic sea-ice variability in recent decades reasonably well. The sea-ice component in the model has an ability to reproduce the well-documented gradual increasing trend in Antarctic sea-ice extent over most of the period and its sudden decrease in the last few years^{41,57}.

Data availability

The JARE hydrographic observation data are available through Arctic Data archive System at NIPR (https://ads.nipr.ac.jp/dataset/A20200518-001_/A20220128-001~-006). Temperature and salinity data of tethered profiler data in 2017 are available at <https://doi.org/10.17592/001.2020051801>. Time-series $\delta^{18}\text{O}$ in 2017 are available at <https://doi.org/10.17592/001.2022012801>. Time series current meter at <https://doi.org/10.17592/001.2022012802>. Time series conductivity and temperature recorder data in 2019 are at <https://doi.org/10.17592/001.2022012803>. Temperature and salinity profiler in 2019 are at <https://doi.org/10.17592/001.2022012804>. CTD data off Cape Darnley during 2010–2020 are at <https://doi.org/10.17592/001.2022012805>. Bottle $\delta^{18}\text{O}$ during 2011–2010 are at <https://doi.org/10.17592/001.2022012806>. XCTD data are available at https://www.jodc.go.jp/jodcweb/JDOSS/index_j.html. MEOP bioglogging data are available at <https://www.seanoe.org/data/00343/45461/>. Hydrographic data are available through WOD through National centers for environmental information, NOAA at https://www.nodc.noaa.gov/OC5/WOD/pr_wod.html. SIC by NSIDC at <https://nsidc.org/data/nsidc/0051>. SST by NOAA OI SST V2 High Resolution Dataset at <https://psl.noaa.gov/data/gridded/data.noaa.oisst.v2.highres.html>. The satellite-derived SIP are available at <http://www.lowtem.hokudai.ac.jp/wwwod/polar-seaflux/>. Numerical model information and results are available at <https://iopscience.iop.org/article/10.1088/1748-9326/ac0de0>.

Code availability

The Python codes and scripts used to analyze the data and to generate the figures are available from the corresponding author on request.

Received: 17 November 2021; Accepted: 16 May 2022;

Published online: 22 June 2022

References

- Rintoul, S. R. The global influence of localized dynamics in the Southern Ocean. *Nature* **558**, 209–218 (2018).
- Pattyn, F. et al. The Greenland and Antarctic ice sheets under 1.5 °C global warming. *Nat. Clim. Change* **8**, 1053–1061 (2018).
- DeConto, R. M. & Pollard, D. Contribution of Antarctica to past and future sea-level rise. *Nature* **531**, 591–597 (2016).
- Rignot, E. et al. Four decades of Antarctic Ice Sheet mass balance from 1979–2017. *Proc. Natl Acad. Sci. USA* **116**, 1095–1103 (2019).
- Jacobs, S. S. & Giulivi, C. F. Large Multidecadal Salinity Trends near the Pacific–Antarctic Continental Margin. *J. Clim.* **23**, 4508–4524 (2010).
- Purkey, S. G. & Johnson, G. C. Global contraction of Antarctic Bottom Water between the 1980s and 2000s*. *J. Clim.* **25**, 5830–5844 (2012).
- Snow, K., Hogg, A. M., Sloyan, B. M. & Downes, S. M. Sensitivity of Antarctic bottom water to changes in surface buoyancy fluxes. *J. Clim.* **29**, 313–330 (2016).
- DeJong, H. B. & Dunbar, R. B. Air-sea CO₂ exchange in the Ross Sea, Antarctica. *J. Geophys. Res. Oceans* **122**, 8167–8181 (2017).
- Arrigo, K. R. Phytoplankton dynamics within 37 Antarctic coastal polynya systems. *J. Geophys. Res.* <https://doi.org/10.1029/2002JC001739> (2003).
- Morrison, A. K., Hogg, A. M., England, M. H. & Spence, P. Warm Circumpolar Deep Water transport toward Antarctica driven by local dense water export in canyons. *Sci. Adv.* **6**, eaav2516 (2020).
- Moorman, R., Morrison, A. K. & McC. Hogg, A. Thermal responses to Antarctic Ice Shelf Melt in an Eddy-Rich Global Ocean–Sea Ice Model. *J. Clim.* **33**, 6599–6620 (2020).
- Ohshima, K. I. et al. Antarctic Bottom Water production by intense sea-ice formation in the Cape Darnley polynya. *Nat. Geosci.* **6**, 235–240 (2013).
- Aoki, S., Ono, K., Hirano, D. & Tamura, T. Continuous winter oceanic profiling in the Cape Darnley Polynya, East Antarctica. *J. Oceanogr.* **76**, 365–372 (2020).
- Tamura, T., Ohshima, K. I. & Nihashi, S. Mapping of sea ice production for Antarctic coastal polynyas. *Geophys. Res. Lett.* **35**, n/a–n/a (2008).
- Fricker, H. A., Young, N. W., Allison, I. & Coleman, R. Iceberg calving from the Amery Ice Shelf, East Antarctica. *Ann. Glaciol.* **34**, 241–246 (2002).
- Smith, N. R., Zhaoqian, D., Kerry, K. R. & Wright, S. Water masses and circulation in the region of Prydz Bay, Antarctica. *Deep Sea Res. Part A. Oceanogr. Res. Pap.* **31**, 1121–1147 (1984).
- Liu, C. et al. Modeling modified Circumpolar Deep Water intrusions onto the Prydz Bay continental shelf, East Antarctica. *J. Geophys. Res. Oceans* **122**, 5198–5217 (2017).
- Williams, G. D. et al. The suppression of Antarctic bottom water formation by melting ice shelves in Prydz Bay. *Nat. Commun.* **7**, 12577 (2016).
- Galton-Fenzi, B. K., Hunter, J. R., Coleman, R., Marsland, S. J. & Warner, R. C. Modeling the basal melting and marine ice accretion of the Amery Ice Shelf. *J. Geophys. Res.* **117**, C09031 (2012).
- Herraz-Borreguero, L. et al. Circulation of modified Circumpolar Deep Water and basal melt beneath the Amery Ice Shelf, East Antarctica. *J. Geophys. Res. Oceans* **120**, 3098–3112 (2015).
- Jacobs, S. S. et al. Melting of ice shelves and the mass balance of Antarctica. *J. Glaciol.* **38**, 375–387 (1992).
- Jenkins, A. et al. Decadal Ocean Forcing and Antarctic Ice Sheet Response: lessons from the Amundsen Sea. *Oceanography* **29**, 106–117 (2016).
- Silvano, A. et al. Freshening by glacial meltwater enhances melting of ice shelves and reduces formation of Antarctic Bottom Water. *Sci. Adv.* **4**, eaap9467 (2018).
- Stewart, C. L., Christoffersen, P., Nicholls, K. W., Williams, M. J. M. & Dowdeswell, J. A. Basal melting of Ross Ice Shelf from solar heat absorption in an ice-front polynya. *Nat. Geosci.* **12**, 435–440 (2019).
- Malyarenko, A., Robinson, N. J., Williams, M. J. M. & Langhorne, P. J. A wedge mechanism for summer surface water inflow into the Ross ice shelf cavity. *J. Geophys. Res. Oceans* **124**, 1196–1214 (2019).
- Huang, B. et al. Improvements of the daily optimum interpolation sea surface temperature (DOISST) version 2.1. *J. Clim.* **34**, 2923–2939 (2021).
- Jacobs, S. S., Fairbanks, R. G. & Horibe, Y. Origin and evolution of water masses near the Antarctic continental margin: evidence from H218O/H216O ratios in sea water. *Oceanol. Antarct. Cont. Shelf Antarct. Res. Ser.* **43**, 59–85 (1985).
- Cavalieri, D. J., Parkinson, C. L., Gloersen, P. and Zwally, H. J. *Sea Ice Concentrations from Nimbus-7 SMMR and DMSP SSM/I-SSMIS Passive Microwave Data* (1996).

29. Ohshima, K. I. & Nishashi, S. A simplified ice–ocean coupled model for the Antarctic ice melt season. *J. Phys. Oceanogr.* **35**, 188–201 (2005).
30. Timmermann, R. et al. A consistent data set of Antarctic ice sheet topography, cavity geometry, and global bathymetry. *Earth Syst. Sci. Data* **2**, 261–273 (2010).
31. Zhou, Q. et al. Wind-driven spreading of fresh surface water beneath ice shelves in the Eastern Weddell Sea. *J. Geophys. Res. Oceans* **119**, 3818–3833 (2014).
32. Ohshima, E. A. Seasonal variations of the Antarctic coastal ocean in the vicinity of Lutzow-Holm Bay. *J. Geophys. Res. Oceans* **101**, 20617–20628 (1996).
33. Wen, J. et al. Basal melting and freezing under the Amery Ice Shelf, East Antarctica. *J. Glaciol.* **56**, 81–90 (2010).
34. Yu, J., Liu, H., Jezek, K. C., Warner, R. C. & Wen, J. Analysis of velocity field, mass balance, and basal melt of the Lambert Glacier–Amery Ice Shelf system by incorporating Radarsat SAR interferometry and ICESat laser altimetry measurements. *J. Geophys. Res.* <https://doi.org/10.1029/2010JB007456> (2010).
35. Rignot, E., Jacobs, S., Mouginot, J. & Scheuchl, B. Ice-shelf melting around Antarctica. *Science* **341**, 266–270 (2013).
36. Spergel, J. J., Kingslake, J., Creyts, T., van Wessem, M. & Fricker, H. A. Surface meltwater drainage and ponding on Amery Ice Shelf, East Antarctica, 1973–2019. *J. Glaciol.* <https://doi.org/10.1017/jog.2021.46> (2021).
37. Turner, J. et al. Unprecedented springtime retreat of Antarctic sea ice in 2016. *Geophys. Res. Lett.* **44**, 6868–6875 (2017).
38. Parkinson, C. L. A 40-y record reveals gradual Antarctic sea ice increases followed by decreases at rates far exceeding the rates seen in the Arctic. *Proc. Natl Acad. Sci. USA* **116**, 14414–14423 (2019).
39. Riihela, A., Bright, R. M. & Anttila, K. Recent strengthening of snow and ice albedo feedback driven by Antarctic sea-ice loss. *Nat. Geosci.* **14**, 832–836 (2021).
40. Stuecker, M. F., Bitz, C. M. & Armour, K. C. Conditions leading to the unprecedented low Antarctic sea ice extent during the 2016 austral spring season. *Geophys. Res. Lett.* **44**, 9008–9019 (2017).
41. Kusahara, K., Reid, P., Williams, G. D., Massom, R. & Hasumi, H. An ocean–sea ice model study of the unprecedented Antarctic sea ice minimum in 2016. *Environ. Res. Lett.* **13**, 84020 (2018).
42. Roach, L. A. et al. Antarctic Sea Ice Area in CMIP6. *Geophys. Res. Lett.* <https://doi.org/10.1029/2019GL086729> (2020).
43. Purich, A. & England, M. H. Historical and future projected warming of Antarctic shelf bottom water in CMIP6 models. *Geophys. Res. Lett.* <https://doi.org/10.1029/2021GL092752> (2021).
44. Kusahara, K. Summertime linkage between Antarctic sea-ice extent and ice-shelf basal melting through Antarctic coastal water masses’ variability: a circumpolar Southern Ocean model study. *Environ. Res. Lett.* **16**, 074042 (2021).
45. Boyer, T. P. et al. *World Ocean Database 2018* (2018).
46. Treasure, A. et al. Marine mammals exploring the oceans pole to pole: a review of the MEOP consortium. *Oceanography* **30**, 132–138 (2017).
47. Jenkins, A. The impact of melting ice on ocean waters. *J. Phys. Oceanogr.* **29**, 2370–2381 (1999).
48. Biddle, L. C., Loose, B. & Heywood, K. J. Upper ocean distribution of glacial meltwater in the Amundsen Sea, Antarctica. *J. Geophys. Res. Oceans* **124**, 6854–6870 (2019).
49. Meredith, M. P. et al. Variability in the freshwater balance of northern Marguerite Bay, Antarctic Peninsula: results from $\delta^{18}\text{O}$. *Deep Sea Res. Part II: Top. Stud. Oceanogr.* **55**, 309–322 (2008).
50. Craig, H. & Gordon, L. I. Stable isotopes in oceanographic studies. Deuterium and oxygen 18 variations in the ocean and the marine atmosphere. *Stable isotopes in oceanographic studies and paleotemperatures*, 9–130 (1965).
51. Tamura, T., Ohshima, K. I., Fraser, A. D. & Williams, G. D. Sea ice production variability in Antarctic coastal polynyas. *J. Geophys. Res. Oceans* **121**, 2967–2979 (2016).
52. Kusahara, K. & Hasumi, H. Modeling Antarctic ice shelf responses to future climate changes and impacts on the ocean. *J. Geophys. Res. Oceans* **118**, 2454–2475 (2013).
53. Roske, F. A global heat and freshwater forcing dataset for ocean models. *Ocean Model.* **11**, 235–297 (2006).
54. Kara, A. B., Rochford, P. A. & Hurlburt, H. E. Efficient and accurate bulk parameterizations of air–sea fluxes for use in general circulation models. *J. Atmos. Ocean. Technol.* **17**, 1421–1438 (2000).
55. Holland, D. M. & Jenkins, A. Modeling thermodynamic ice–ocean interactions at the base of an ice shelf. *J. Phys. Oceanogr.* **29**, 1787–1800 (1999).
56. Hellmer, H. H. & Olbers, D. J. A two-dimensional model for the thermohaline circulation under an ice shelf. *Antarct. Sci.* **1**, 325–336 (1989).
57. Kusahara, K., Williams, G. D., Massom, R., Reid, P. & Hasumi, H. Spatiotemporal dependence of Antarctic sea ice variability to dynamic and thermodynamic forcing: a coupled ocean–sea ice model study. *Clim. Dyn.* **52**, 3791–3807 (2019).

Acknowledgements

We are grateful to Dr. M. Kawai for supporting RAS-500 observation and to Ms. M. Kitagawa for conducting $\delta^{18}\text{O}$ analysis. This work was supported by Grants-in-Aids for Scientific Research (JP17H06316, JP17H06317, JP17H06322, JP17H06323, JP17H04710, JP19K12301, JP21H04918, and JP21H04931) of the Ministry of Education, Culture, Sports, Science and Technology, the Science Program of Japanese Antarctic Research Expedition (JARE) as Prioritized Research Project, National Institute of Polar Research (NIPR) through Project Research KP-303, the Center for the Promotion of Integrated Sciences of SOKENDAI, and the Joint Research Program of the Institute of Low Temperature Science, Hokkaido University.

Author contributions

S.A. and Tomoki Takahashi conceived this study. S.A., K.Y., D.H., K.O., and Takeshi Tamura designed and conducted oceanographic observations onboard Shirase. K.K. developed the numerical model. Tomoki Takahashi, D.H., and K.Y. analyzed the hydrographic and satellite observation data and numerical model data. S.A., G.W., and K.Y. wrote the paper, and all authors discussed the results and commented on the manuscript.

Competing interests

The authors declare no competing interests.

Additional information

Supplementary information The online version contains supplementary material available at <https://doi.org/10.1038/s43247-022-00456-z>.

Correspondence and requests for materials should be addressed to Shigeru Aoki.

Peer review information *Communications Earth & Environment* thanks the anonymous reviewers for their contribution to the peer review of this work. Primary Handling Editors: Jan Lenaerts, Heike Langenberg. Peer reviewer reports are available.

Reprints and permission information is available at <http://www.nature.com/reprints>

Publisher’s note Springer Nature remains neutral with regard to jurisdictional claims in published maps and institutional affiliations.



Open Access This article is licensed under a Creative Commons Attribution 4.0 International License, which permits use, sharing, adaptation, distribution and reproduction in any medium or format, as long as you give appropriate credit to the original author(s) and the source, provide a link to the Creative Commons license, and indicate if changes were made. The images or other third party material in this article are included in the article’s Creative Commons license, unless indicated otherwise in a credit line to the material. If material is not included in the article’s Creative Commons license and your intended use is not permitted by statutory regulation or exceeds the permitted use, you will need to obtain permission directly from the copyright holder. To view a copy of this license, visit <http://creativecommons.org/licenses/by/4.0/>.

© The Author(s) 2022